




Cite this: *Inorg. Chem. Front.*, 2022, **9**, 1406

Dual-functional ratiometric fluorescent sensor based on mixed-lanthanide metal–organic frameworks for the detection of trace water and temperature†

Xiaoyong Zhai,^a Pengfei Feng,^a Nan Song,^a Guodong Zhao,^a Qingyi Liu,^a Liangliang Liu,^{*a} Mei Tang^b and Yu Tang ^{*a,c}

Rapid-response ratiometric sensors are promising tools to detect trace water and temperature. However, achieving an accurately visualized water assay in a very narrow range is still a challenge. Herein, a novel dual-functional ratiometric luminescent sensor, *i.e.*, Eu_{2.2}Tb_{97.8}-TCA, was successfully fabricated based on lanthanide metal–organic frameworks. This sensor showed a very fast (less than 20 s) and relatively ultrasensitive (limit of detection 0.016% v/v) response to trace water in ethanol, achieving the sensitive visual determination of water in ethanol with multiple readouts. Intriguingly, visual and quantitative determination of water with a detection limit of 0.035% v/v was achieved based on the ratio of green (G) to red (R) values combined with a smartphone color picker application (APP). The mechanism has also been proposed based on experimental and theoretical evaluation. Furthermore, Eu_{2.2}Tb_{97.8}-TCA could monitor temperature in the range of 300 to 380 K with an excellent linear relationship, high accuracy and good recyclability. This material could also be tuned to emit white luminescence and hence can be used as a single-phase UV phosphor. The present work provides a novel Ln-MOF with powerful capabilities to detect trace water and monitor temperature, which paves a way for the rational design and synthesis of multifunctional materials.

Received 11th January 2022,
Accepted 8th February 2022

DOI: 10.1039/d2qi00093h

rs.c.li/frontiers-inorganic

1. Introduction

Water content and temperature are two very crucial factors because even minor changes in water content or temperature will definitely affect reaction efficiency and even threaten laboratory safety not only in micro-reactions but also in industrial production. As far as organic solvents are concerned, trace water is treated as one of the most pervasive impurities, which is difficult to solve in laboratory settings and in the chemical industry.^{1,2} Therefore, it is quite necessary to develop simple, reliable, and fast sensors for water detection in organic solvents. Traditionally, Karl Fischer titration and gas chromatography

are broadly used for the detection of water content. However, both these techniques have certain limitations, such as the requirement of costly instruments, long detection time, specialized personnel, and incompetency in the real-time and *in situ* determination of water content.³ To get around these limitations, much attention has been paid to developing luminescent detectors for sensing water.^{4,5} Compared with traditional analytical methods, luminescent water sensors featuring ease of fabrication, simple operation, high sensitivity, fast response, and capability for *in situ* and non-invasive determination may serve as promising alternatives.^{4,6,7} Recently, a few fluorescent materials have been developed to determine water content, such as organic fluorescent molecules,^{8,9} polymers,¹⁰ metal complexes,¹¹ copper clusters,^{12,13} carbon dots,^{14,15} lanthanide hybrids,^{16,17} up-conversion nanoparticles,^{18,19} and Ln-MOFs.^{5,20–25} Most of these water sensors can be applied to monitor water content in a relatively broad linear range (0%–*x* % v/v, *x* > 0.7). However, developing an accurately visualized water assay in the narrow linear range (0%–0.7% v/v) of water content commonly found in analytical pure chemical reagents still remains a challenge.

As for temperature monitoring, many new methods and temperature sensors have been developed, such as liquid-filled

^aState Key Laboratory of Applied Organic Chemistry, Key Laboratory of Nonferrous Metal Chemistry and Resources Utilization of Gansu Province, College of Chemistry and Chemical Engineering, Lanzhou University, Lanzhou 730000, P.R. China. E-mail: tangyu@lzu.edu.cn, liull@lzu.edu.cn

^bDepartment of Rheumatology and Immunology, Second Affiliated Hospital of Soochow University, Suzhou 215004, P.R. China

^cState Key Laboratory of Baiyuanob Rare Earth Resource Researches and Comprehensive Utilization, Baotou Research Institute of Rare Earths, Baotou 014030, P.R. China

†Electronic supplementary information (ESI) available. See DOI: 10.1039/d2qi00093h

glass thermometers, thermocouples and optical sensors.^{26,27} Compared with conventional temperature sensors, luminescence-based thermometers have attracted considerable attention due to their good accuracy, high spatial resolution and fast response. Moreover, they are capable of working in fast-moving objects, in biological fluids without contact and even strong electromagnetic fields.^{28–31} Such temperature determination methods are mainly based on temperature-dependent variation in the luminescence intensity and/or the lifetime of one transition.^{32,33} Some thermometers based on Ln-MOFs,^{30,34,35} luminescent guest-encapsulated MOFs,^{36,37} lanthanide-doped phosphors,^{38,39} up-conversion nanomaterials,^{40,41} and lanthanide-doped micro/nanocrystals,⁴² have been reported. To achieve the simultaneous detection of both trace water and temperature, multifunctional ratiometric fluorescent sensors with good stability, rapid response, high sensitivity and low limit of detection should be developed.

Most notably, Ln-MOFs have drawn great attention and are emerging as prospective ratiometric sensors due to their high color purity, sharp characteristic emission peaks, non-overlapping spectra, and large Stokes shifts.²⁴ Moreover, Ln-MOFs are endowed with more than one emission center that originates from the lanthanide ions or clusters and organic linkers without additional materials.^{43,44} Thus, some ratiometric sensors based on Ln-MOFs exhibit outstanding performance in sensing trace water owing to their simple operation, fast response, low detection limit, and even naked-eye detection.^{5,20–25,45} Further, wide-range temperature sensing and white-light emission can be achieved by adjusting the composition of a family of mixed Ln-MOFs.^{28,29,46} To the best of our knowledge, there are only a few reports on the highly sensitive *in situ* and real-time detection of water content in organic solvents accompanied by a rich and distinct change in the emission color within a narrow linear range. Furthermore, white-light-emitting mixed Ln-MOFs with the same composition ratio capable of sensing both water content and temperature have never been explored. Thus, it is of high necessity to further design and synthesize novel and multifunctional Ln-MOF sensors with excellent performance and discover some new sensing mechanisms.

Herein, a white-light-emitting mixed-lanthanide MOF (Eu_{2.2}Tb_{97.8}-TCA) was developed and utilized as a dual-functional ratiometric luminescent sensor for both trace water monitoring in ethanol and wide-range temperature sensing in the solid state. By comparing the performance in water detection and temperature measurement, Eu_{2.2}Tb_{97.8}-TCA was selected as the ideal material for subsequent research (Fig. S2–S5†). To construct Eu_{2.2}Tb_{97.8}-TCA, Tb³⁺ and Eu³⁺ were chosen as the lanthanide luminescent centers owing to their long fluorescent lifetime and good monochromaticity; 4,4',4''-nitrilotribenzoic acid (H₃TCA) was used to sensitize the lanthanides and probably form coordination bonds *via* the nitrogen atoms. The synthetic route and design strategy are shown in Scheme 1. In this MOF, the ligand and two lanthanides formed multiple emitting centers, and all of them had

different sensitivities toward water and temperature. On the one hand, as the water content increased from 0% to 0.63% v/v, the luminescence intensity of Eu_{2.2}Tb_{97.8}-TCA increased at 544 nm and decreased at 614 nm, and their ratio (I_{544}/I_{614}) *versus* water content showed a good relationship. The water-induced ratiometric luminescence response made the sensor exhibit a distinguishable color transition, which was favorable for naked-eye detection. Thus, sensitive *in situ* and real-time water sensing in ethanol could be implemented through multiple readouts involving emission color, ratiometric luminescence intensity, Commission International d'Éclairage (CIE) chromaticity diagram, and a smartphone-based color picking system. Furthermore, this work demonstrated an infrequent hydrogen-bond mechanism in Ln-MOFs for sensing water content, which provides a new perspective for developing water sensors based on Ln-MOFs. On the other hand, Eu_{2.2}Tb_{97.8}-TCA could be used for wide-range temperature determination. Based on its white-light emission at elevated temperatures, it can also serve as a promising single-phase phosphor material, thus providing a new option for fabricating ultraviolet white-light-emitting diodes (WLED).

2. Experimental details

2.1. Synthesis of Eu/Gd-TCA

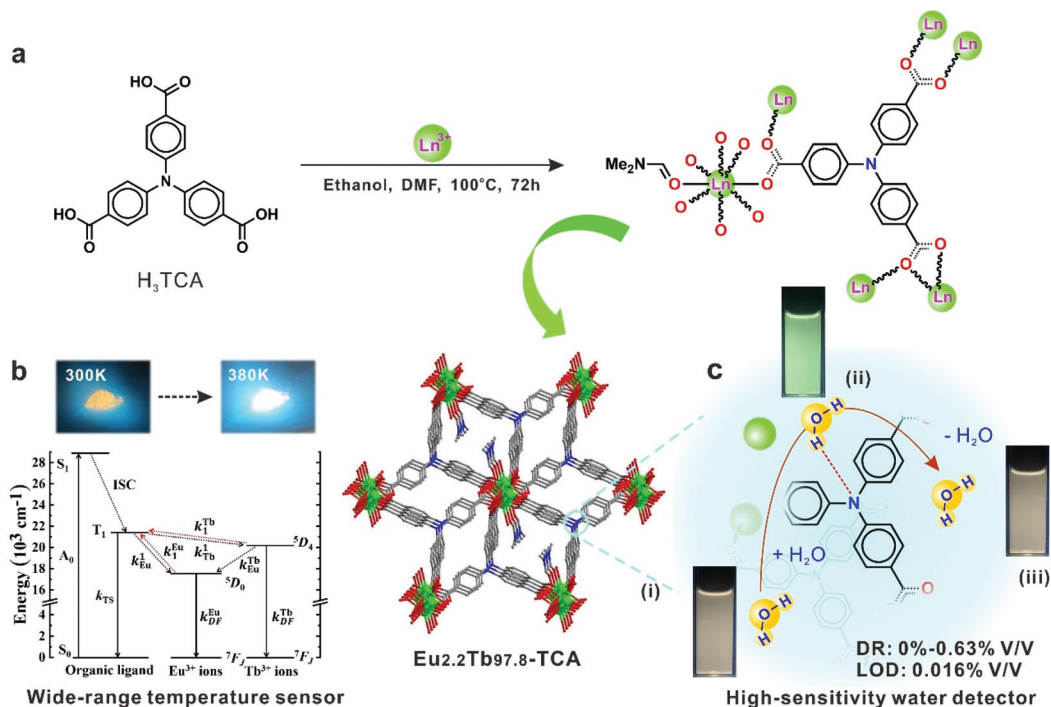
The synthetic route of the ligand, namely H₃TCA, is given in the ESI.† Eu-TCA and Gd-TCA were prepared according to a method described in previous work.⁴⁷ Eu(NO₃)₃·6H₂O (44.6 mg, 0.10 mmol) and H₃TCA (41.5 mg, 0.11 mmol) were added in DMF (3 mL) and ethanol (3 mL). The mixture was heated at 100 °C for three days and a pale-yellow powder of Eu-TCA was obtained. Similarly, Gd-TCA was synthesized as an off-white powder by using Gd(NO₃)₃·6H₂O as the lanthanide salt.

2.2. Synthesis of Eu_{2.2}Tb_{97.8}-TCA

To a mixture of Eu(NO₃)₃·6H₂O (1.3 mg, 0.003 mmol), Tb(NO₃)₃·6H₂O (43.9 mg, 0.097 mmol) and H₃TCA (41.5 mg, 0.11 mmol) were added in DMF (3 mL) and ethanol (3 mL). The mixture was heated at 100 °C for three days and the pale-yellow powder of Eu_{2.2}Tb_{97.8}-TCA was obtained.

2.3. Trace water detection in ethanol

Prior to PL spectroscopy, Eu_{2.2}Tb_{97.8}-TCA was soaked in fresh dry ethanol for 24 h, and the solvent was wiped off under a vacuum condition. The activated powder (3.0 mg) was added to dried ethanol (10 mL), and this mixture was sonicated for 10 minutes to form a suspension. Then, the suspension (3 mL) was transferred to a cuvette immediately. The original PL spectrum was collected prior to the addition of a certain amount of water. Afterwards, a set amount of water was gradually added to the suspension and whirled for 10 seconds, and then, PL spectra were collected. The water concentration was accurately controlled by using a microsyringe (5 μL). Additionally, the determination method of the intensity ratio (I_{544}/I_{614}) was based on the peak value.



Scheme 1 Schematic illustration of the synthetic route and design strategy of $\text{Eu}_{2.2}\text{Tb}_{97.8}\text{-TCA}$ used for highly efficient water detection and temperature sensing. DR: detection range; LOD: limit of detection.

2.4. Sensing of temperature in the solid state

The newly synthesized $\text{Eu}_{2.2}\text{Tb}_{97.8}\text{-TCA}$ powder was packaged into the sample tank of Horiba Instruments FL-3. The temperature-dependent luminescence spectra were measured upon heating to a certain temperature and maintaining it for 10 minutes, respectively.

3. Results and discussion

3.1. Structure of Ln-TCA MOFs

Ln-TCA was prepared by the hydrothermal reaction of H_3TCA and the corresponding lanthanide salt (Scheme 1). The powder X-ray diffraction (PXRD) patterns of the obtained Ln-TCA are shown in Fig. 1a, and it was found that the newly synthesized Ln-TCA matched well with the simulated one, implying the successful synthesis of MOFs.⁴⁷ According to the Fourier transform infrared (FTIR) spectra in Fig. S6,[†] the characteristic peaks of C=O and C=C in H_3TCA had shifted respectively from 1721 and 1684 cm^{-1} to 1675 and 1633 cm^{-1} , indicating the coordination of the ligand and the lanthanide center. Besides, the absorption peaks of Ln-TCA displayed a bathochromic shift in the range of 300–450 nm compared with H_3TCA , confirming efficient coordination (Fig. 1b). The molar ratio of Eu^{3+} to Tb^{3+} in the bimetallic lanthanide MOF was determined to be 2.2:97.8 by inductively coupled plasma atomic emission spectroscopy (ICPs) and was further confirmed by Energy Dispersive X-ray (EDX) spectroscopy (Fig. S7

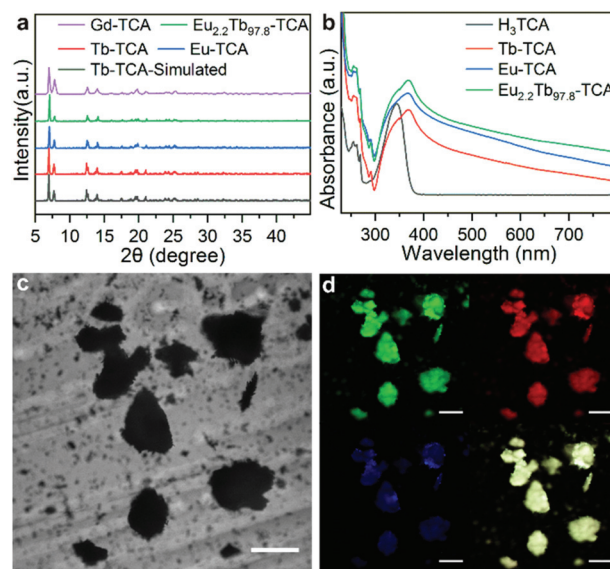


Fig. 1 (a) The PXRD patterns of Tb-TCA-simulated, Tb-TCA, Eu-TCA, $\text{Eu}_{2.2}\text{Tb}_{97.8}\text{-TCA}$ and Gd-TCA. (b) UV-vis absorption spectra of H_3TCA , Tb-TCA, Eu-TCA, and $\text{Eu}_{2.2}\text{Tb}_{97.8}\text{-TCA}$. (c) and (d) Confocal laser scanning microscopy images of $\text{Eu}_{2.2}\text{Tb}_{97.8}\text{-TCA}$, under the same excitation; the fluorescence emitted in the different luminescence channels were collected to visualize the fluorescent colors of the multiple emission centers and their merger. Green for Tb^{3+} , red for Eu^{3+} , blue for ligand and pale yellow for merger. All scale bars: 200 μm .

and Table S1†). Furthermore, a lumpy morphology was observed for $\text{Eu}_{2.2}\text{Tb}_{97.8}\text{-TCA}$ from the scanning electron microscopic (SEM) images (Fig. S8†). Meanwhile, the scanning transmission electron microscopic (STEM) images and energy dispersive spectroscopy (EDS) elemental mapping images of $\text{Eu}_{2.2}\text{Tb}_{97.8}\text{-TCA}$ demonstrated that Eu^{3+} and Tb^{3+} were uniformly distributed in each particle (Fig. S9†).

3.2. Stability of $\text{Eu}_{2.2}\text{Tb}_{97.8}\text{-TCA}$

The thermogravimetric analysis (TGA) demonstrated that $\text{Eu}_{2.2}\text{Tb}_{97.8}\text{-TCA}$ was thermodynamically stable when the temperature was elevated until about 210 °C, while the crystalline framework started to decompose at higher temperatures (Fig. S10†). After immersing $\text{Eu}_{2.2}\text{Tb}_{97.8}\text{-TCA}$ in dried ethanol for 12 h and the experiment of water detection, the PXRD patterns had no change, revealing that this material was stable in dried ethanol and the process of water determination (Fig. S11†). Upon raising the temperature to 380 K and then cooling to 300 K, the structure of $\text{Eu}_{2.2}\text{Tb}_{97.8}\text{-TCA}$ was intact (Fig. S12†). These results suggested that $\text{Eu}_{2.2}\text{Tb}_{97.8}\text{-TCA}$ might have the potential to be utilized as a luminescent sensor.

3.3. Photoluminescence properties

The excitation spectra of Eu-TCA and Tb-TCA , as control samples, were measured both in the solid state and the dispersion of ethanol, and the maximum excitation wavelengths were 350 and 365 nm, respectively (Fig. S13†). As depicted in Fig. S14,† the solid luminescence spectra of H_3TCA , Eu-TCA , Tb-TCA and $\text{Eu}_{2.2}\text{Tb}_{97.8}\text{-TCA}$ were collected at room temperature. Upon excitation at 350 nm, free H_3TCA showed a strong emission at 435 nm, Eu-TCA showed characteristic transitions ($^5\text{D}_0\text{-}^7\text{F}_j, J = 1\text{-}4$) of Eu^{3+} at 591, 616, 651 and 698 nm, and Tb-TCA also exhibited characteristic transitions ($^5\text{D}_4\text{-}^7\text{F}_j, J = 6\text{-}3$) of Tb^{3+} at 488, 544, 583 and 620 nm. The luminescence behaviors of Tb-TCA and Eu-TCA indicated that Tb^{3+} and Eu^{3+} could be sensitized by H_3TCA based on the antenna effect. As expected, the characteristic transitions of Eu^{3+} and Tb^{3+} existed in the emission spectrum of $\text{Eu}_{2.2}\text{Tb}_{97.8}\text{-TCA}$. As shown in the CIE chromaticity diagram (Fig. S15†), the fluorescent color coordinates of all the luminescent materials mentioned above were present. Moreover, in the confocal laser scanning microscopic (CLSM) images, multiple emission centers formed by the lanthanide ions and the organic ligand displayed their corresponding fluorescent colors, and $\text{Eu}_{2.2}\text{Tb}_{97.8}\text{-TCA}$ comprehensively emitted yellow fluorescence (Fig. 1c and d), testifying that the red emission of Eu^{3+} was dominant in $\text{Eu}_{2.2}\text{Tb}_{97.8}\text{-TCA}$.

3.4. Detection of trace water in ethanol

Upon excitation at 365 nm, the suspensions of Eu-TCA and Tb-TCA exhibited their characteristic transitions, respectively. With increasing water content, the luminescence intensity of Tb^{3+} in Tb-TCA enhanced gradually, whereas the luminescence intensity of Eu^{3+} in Eu-TCA decreased (Fig. 2a and b, Fig. S16†). This suggested that H_3TCA had higher energy transition efficiency (E) toward Tb^{3+} than Eu^{3+} with the addition of

water. Then, $\text{Eu}_{2.2}\text{Tb}_{97.8}\text{-TCA}$ was prepared as a ratiometric sensor to quantify the water content. $\text{Eu}_{2.2}\text{Tb}_{97.8}\text{-TCA}$ showed the characteristic sharp peaks of Tb^{3+} and Eu^{3+} with different volumes of water ranging from 0.0% to 0.9% (Fig. 2c) upon excitation with the light at 365 nm. Similar to the fluorescence behaviors of Tb-TCA and Eu-TCA , the luminescence intensity of $\text{Eu}_{2.2}\text{Tb}_{97.8}\text{-TCA}$ enhanced at 544 nm and decreased at 614 nm (Fig. 2d). When in contact with trace water, the luminescent colors changed rapidly in a few seconds owing to the hydrophilic cavity of $\text{Eu}_{2.2}\text{Tb}_{97.8}\text{-TCA}$.²⁴

The color of $\text{Eu}_{2.2}\text{Tb}_{97.8}\text{-TCA}$ in suspension gradually changed from white to yellowish green and green, which could be visualized under illumination by UV-light at 365 nm after titration with trace water and was also confirmed by the corresponding CIE coordinates (Fig. 2e). Therefore, the good correlation between the standard CIE coordinates inspired us to develop a new read-in and read-out method to precisely quantify the water content (Table S2†). Additionally, the ratio of emission intensities (I_{544}/I_{614}) 544 nm and 614 nm wavelengths exhibited an excellent S-shape response towards water content in the range of 0%–0.9% v/v (Fig. 2f), showing a good piecewise linear relationship and fitting well with the equations (Fig. 2g and h). $\text{Eu}_{2.2}\text{Tb}_{97.8}\text{-TCA}$ proved to be a sensitive detector of trace water in ethanol with a very low LOD of 0.016% v/v according to the $3\delta/\text{slope}$, which could be ascribed to preconcentration of water molecules within the channels of the MOFs. As shown in Table S3,† compared with other reported water sensors composed of MOFs, $\text{Eu}_{2.2}\text{Tb}_{97.8}\text{-TCA}$ possessed a relatively low LOD, and the detection was limited to a very narrow range. The previously reported sensors for trace water with LODs below 0.016% v/v did not have such a narrow detection range. Significantly, the rich and distinguishable color transition within such a narrow range was beneficial to the visual analysis of trace water in ethanol. Besides, no obvious change in the emission intensity ratio (I_{544}/I_{614}) was observed after three alternative cycles where $\text{Eu}_{2.2}\text{Tb}_{97.8}\text{-TCA}$ was dispersed in ethanol and ethanol containing 0.63% v/v water, confirming the good reversibility of this self-calibrated luminescent sensor (Fig. 2i).

3.5. The water detection mechanism of $\text{Eu}_{2.2}\text{Tb}_{97.8}\text{-TCA}$

To explore the possible mechanism of water detection, certain favorable factors were investigated. Firstly, the luminescent lifetimes of the lanthanide ions were investigated at different water contents (Fig. S17†). $\text{Eu}_{2.2}\text{Tb}_{97.8}\text{-TCA}$ exhibited a shorter $^5\text{D}_4$ (Tb^{3+}) lifetime than Tb-TCA but longer $^5\text{D}_0$ (Eu^{3+}) lifetime than Eu-TCA at the same water content (Fig. S18†) due to the intermetallic energy transition from Tb^{3+} to Eu^{3+} . Then, the lifetimes of Tb^{3+} ($^5\text{D}_4$) in Tb-TCA , Eu^{3+} ($^5\text{D}_0$) in Eu-TCA , and those in $\text{Eu}_{2.2}\text{Tb}_{97.8}\text{-TCA}$ at different amounts of D_2O (0%–0.9% v/v) were measured (Fig. S19†). We found that they displayed similar lifetime variation tendency but longer lifetimes in the D_2O system than in the H_2O system (Fig. S20†); this is because the O–D oscillators are less effective at vibronic quenching than the corresponding O–H oscillators.⁴⁸ Thus, it could be preliminarily concluded that the lifetime variations

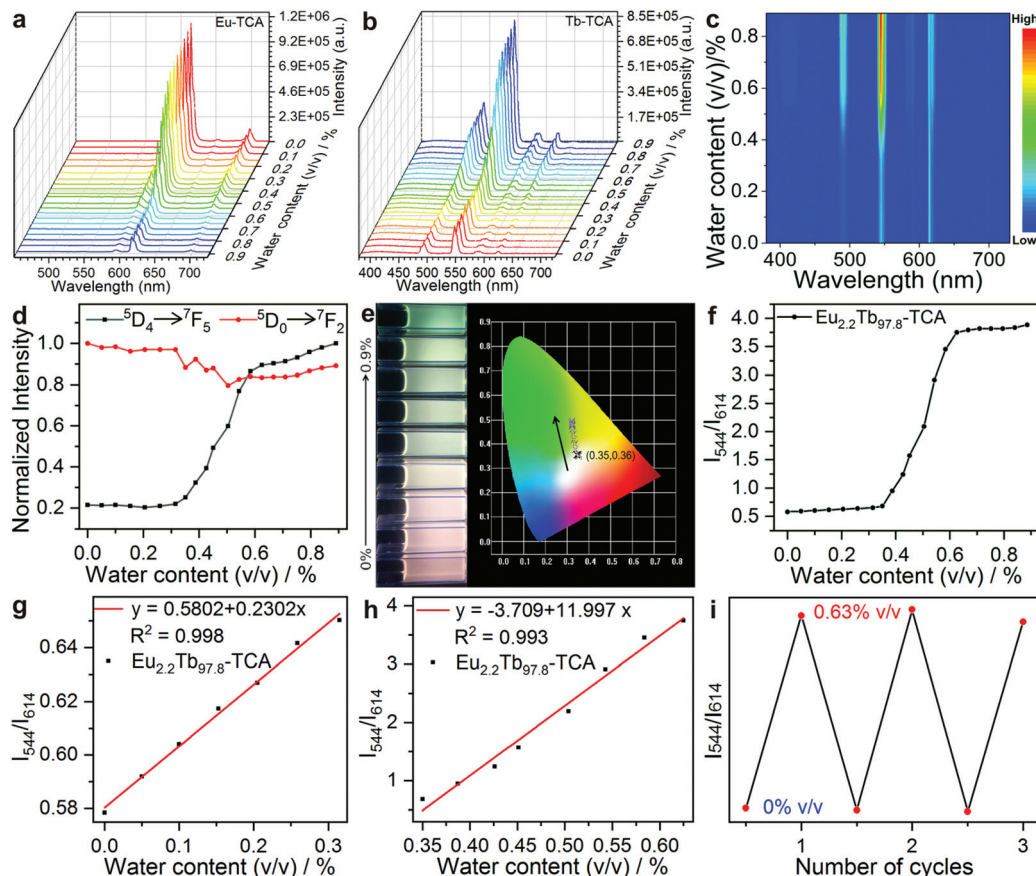


Fig. 2 The fluorescence spectra of (a) Eu-TCA and (b) Tb-TCA recorded at different water contents in ethanol. (c) Color-coded contour map showing the fluorescence spectra of $\text{Eu}_{2.2}\text{Tb}_{97.8}\text{-TCA}$ at different water contents. (d) The ${}^5\text{D}_4 \rightarrow {}^7\text{F}_5$ and ${}^5\text{D}_0 \rightarrow {}^7\text{F}_2$ transitions of $\text{Eu}_{2.2}\text{Tb}_{97.8}\text{-TCA}$ at different water contents. (e) CIE chromaticity diagram showing the fluorescent color coordinates and optical photos showing the color variation of the $\text{Eu}_{2.2}\text{Tb}_{97.8}\text{-TCA}$ ethanol dispersions (0.3 mg mL^{-1}) in the range of 0%–0.9% v/v water. (f) Normalized fluorescence intensity ratio (I_{544}/I_{614}) versus water content. (g) and (h) Normalized fluorescence intensity ratio (I_{544}/I_{614}) versus water content calibration curves in different ranges. (i) Reversible changes in the relative emission intensities I_{544}/I_{614} of $\text{Eu}_{2.2}\text{Tb}_{97.8}\text{-TCA}$ during cycles of alternate immersion in dried ethanol and ethanol containing 0.63% v/v water.

in $\text{Eu}_{2.2}\text{Tb}_{97.8}\text{-TCA}$ might be caused by the interaction between the MOF and water molecules.

It is noteworthy that the coordination number of the lanthanide ions was eight or nine; thus we speculated that they would further coordinate with the adsorbed water molecules. To verify this hypothesis, the number of water molecules in the first coordination sphere of Eu^{3+} in Eu-TCA and Tb^{3+} in Tb-TCA, and those in $\text{Eu}_{2.2}\text{Tb}_{97.8}\text{-TCA}$ were estimated, respectively, by using the following equation (Fig. S21[†]),⁴⁸

$$q = 1.2(\tau_{\text{H}}^{-1} - \tau_{\text{D}}^{-1} - 0.25),$$

where q represents the number of coordinated water molecules, and τ_{H} and τ_{D} are the luminescent lifetimes measured in H_2O and D_2O , respectively. In Table S4,[†] the calculated values of q for different materials are listed in detail. As a consequence, some water molecules had to be removed to match the energy transfer process in the lanthanide ions, whereas the number of coordinated water molecules did not decrease with

the addition of water. Additionally, the organic solvents accommodated in the cavities were gradually replaced by water molecules owing to their smaller size and low steric hindrance, leading to an environment surrounded by water for the H_3TCA linkers. Therefore, we speculated that the variations in the emission spectra of $\text{Eu}_{2.2}\text{Tb}_{97.8}\text{-TCA}$ were the result of the interaction between the adsorbed water molecules and the linkers of MOFs instead of the lanthanide ions.

Furthermore, the phosphorescence spectra of Gd-TCA dispersed in dried ethanol and ethanol containing 0.63% v/v water were investigated. The triplet energy level (T_1) of H_3TCA was obtained at 21053 cm^{-1} (475 nm) and 21598 cm^{-1} (463 nm) (Fig. S22[†]). The results indicated that the emission band of Gd-TCA dispersed in ethanol containing 0.63% v/v water had a hypochromatic shift with a difference of 12 nm, and it could also be illustrated by the UV-vis absorption spectra of Gd-TCA in different cases (Fig. S23[†]). These phenomena suggested that the adsorbed water molecules could enhance the T_1 energy of the ligand. Further, on the

basis of Latva's rule, the energy difference (ΔE) in the most suitable energy transfer process from the ligand to the metal must be 2500–4000 cm^{-1} for Eu^{3+} ($^5\text{D}_0$) and 2500–4500 cm^{-1} for Tb^{3+} ($^5\text{D}_4$).²⁵ The emission of the strongest transitions of Eu^{3+} ($^5\text{D}_0 \rightarrow ^7\text{F}_2$) and Tb^{3+} ($^5\text{D}_4 \rightarrow ^7\text{F}_5$) were at 17 300 and 20 500 cm^{-1} , respectively. Thus, the ΔE between the T_1 of H_3TCA and Ln^{3+} were respectively 3753 and 553 cm^{-1} for Eu^{3+} and Tb^{3+} in dried ethanol, while they were 4298 and 1098 cm^{-1} in ethanol containing 0.63% v/v water. Additionally, the luminescence quantum yields of Eu-TCA and Tb-TCA were also measured in dried ethanol and ethanol containing 0.63% v/v water, respectively. As shown in Fig. S24,[†] the quantum yield of Eu-TCA decreased from 0.3% to 0.28%, whereas that of Tb-TCA increased from 4.51% to 21.7%. These results clearly suggested that the intramolecular energy transfer process from H_3TCA to Tb^{3+} ($^5\text{D}_4$) was more efficient than that to Eu^{3+} ($^5\text{D}_0$) with the addition of water.

Besides, quantum chemical calculations were used to further explore the fluorescence mechanism of $\text{Eu}_{2.2}\text{Tb}_{97.8}\text{-TCA}$ for water sensing. The frontier orbital maps of H_3TCA bonded and not bonded to water were plotted, and the Lowest Unoccupied Molecular Orbital (LUMO) and Highest Occupied Molecular Orbital (HOMO) were calculated (Fig. S25[†]). The energy gap between the LUMO and HOMO of H_3TCA not bonded to water was 3.9752 eV, whereas that of H_3TCA bonded to water was 4.15096 eV. An energy difference of 0.176 eV (13 nm) was observed, which is close to the aforementioned experimental value, indicating that the adsorbed water molecules could enhance the T_1 energy of the ligand *via* coordination bonds, further increasing the energy transfer from H_3TCA to Tb^{3+} and boosting the fluorescence intensity of Tb^{3+} .

Based on the above discussions, we affirmed that this unusual phenomenon may have originated from the hydrogen

bonds formed by the water molecules and the nitrogen atoms of the ligand, which enhance the T_1 energy of the ligand in the $\text{Eu}_{2.2}\text{Tb}_{97.8}\text{-TCA}$ suspension. The energy transition efficiency (E) from T_1 of the ligand to Tb^{3+} ($^5\text{D}_4$) enhanced but that to Eu^{3+} ($^5\text{D}_0$) decreased.

3.6. Visual quantification of trace water

Nowadays, the real-time and rapid detection of trace water is still immature owing to certain limitations of the instruments and the complicated operational procedures. However, it is critical to conduct real-time and on-site inspection of water content. To establish the potential of this sensor in practical application, a smartphone-based color picking system was directly used for water detection in this study. After adding the probes into centrifugal tubes, the equipment could be used to carry out the visual detection of water. Fig. 3a illustrates the information scanning process of $\text{Eu}_{2.2}\text{Tb}_{97.8}\text{-TCA}$ under UV light. The photographs acquired under the illumination of a portable UV lamp (365 nm) could be processed in the RGB color space with a smartphone app (Color Picker). Notably, the material in the centrifuge tubes exhibited a distinct change in emission color from light red to yellowish-green and green upon increasing the water content. There was a good piecewise linear relationship between the G/R values corresponding to the color signals and the water content (0%–0.67% v/v), with a detection limit of 0.035% v/v (Fig. 3b). Meanwhile, they also fitted well with the equations. More importantly, the ratio of G/R values *versus* water content exhibited an excellent S-shape response when the water content was in the range of 0%–0.9% v/v, and the variation tendency was consistent with the result obtained in suspension, as mentioned above. Furthermore, by using probe-loaded centrifugal tubes and a smartphone platform, we realized visual quantification of water content. These

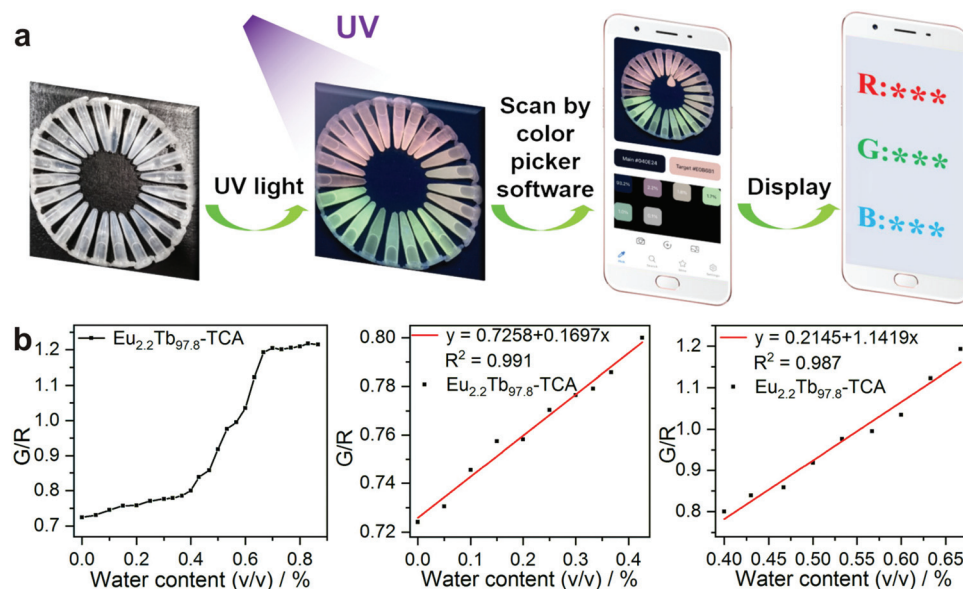


Fig. 3 (a) Photographs of the information scanning process from the $\text{Eu}_{2.2}\text{Tb}_{97.8}\text{-TCA}$ suspensions using the APP. (b) G/R value *versus* water content curve and the calibration curves in different ranges.

results verified that the smart color recognition system can be used for on-site and real-time determination of water content.

3.7. Sensing of temperature

Besides the precise detection of trace water, $\text{Eu}_{2.2}\text{Tb}_{97.8}\text{-TCA}$ also exhibited good performance in temperature monitoring, achieving dual-sensing toward trace water and temperature using two states of a single material and relieving the heavy process of sample preparation. Upon increasing the temperature, the luminescence intensity of both Tb^{3+} and Eu^{3+} reduced progressively, and the intensity of Tb^{3+} declined more slowly than that of Eu^{3+} (Fig. 4a and b, Fig. S26†). It has been observed that single-color fluorescence detection does not afford very accurate measurements due to poor linear relationships and environmental influence.²⁴ Thus, a ratiometric fluorescent sensor was urgently needed. To tentatively evaluate the sensing performance of $\text{Eu}_{2.2}\text{Tb}_{97.8}\text{-TCA}$ as a self-calibrated luminescent thermometer, the temperature-dependent luminescence performance was investigated by raising the temperature from 300 to 380 K (Fig. 4c). As shown in Fig. 4d, the emission intensity of both Tb^{3+} and Eu^{3+} gradually

decreased, and the ratio of the luminescence intensities (I_{544}/I_{616}) versus temperature showed an excellent linear relationship, which fitted well with the equation (Fig. 4e). The CIE coordinates of the fluorescence spectra of $\text{Eu}_{2.2}\text{Tb}_{97.8}\text{-TCA}$ dependent on temperature indicated that the calculated chromaticity gradually move from yellow to white (Fig. S27†). It was also found that the temperature correlated with the color coordinates in the standard CIE chromaticity diagram. Thus, the rich color coordinates could be used to precisely determine the temperature ranging from 300 to 380 K, as displayed in Table S5.† In addition, the performance of a thermometer can be measured by the relative sensitivity (S_r).³⁴ As for $\text{Eu}_{2.2}\text{Tb}_{97.8}\text{-TCA}$, the maximum S_r was determined to be 3.01%/K at 300 K according to the following equation (Fig. 4f), which is superior to those of some other thermometers.^{36,49,50}

$$S_r = \frac{1}{\Delta} \left(\frac{\partial \Delta}{\partial T} \right)$$

where Δ represents the fluorescence intensity ratio of the two transitions (I_{544}/I_{616}). Herein, cycling experiments were also conducted by alternating between 300 and 380 K, which

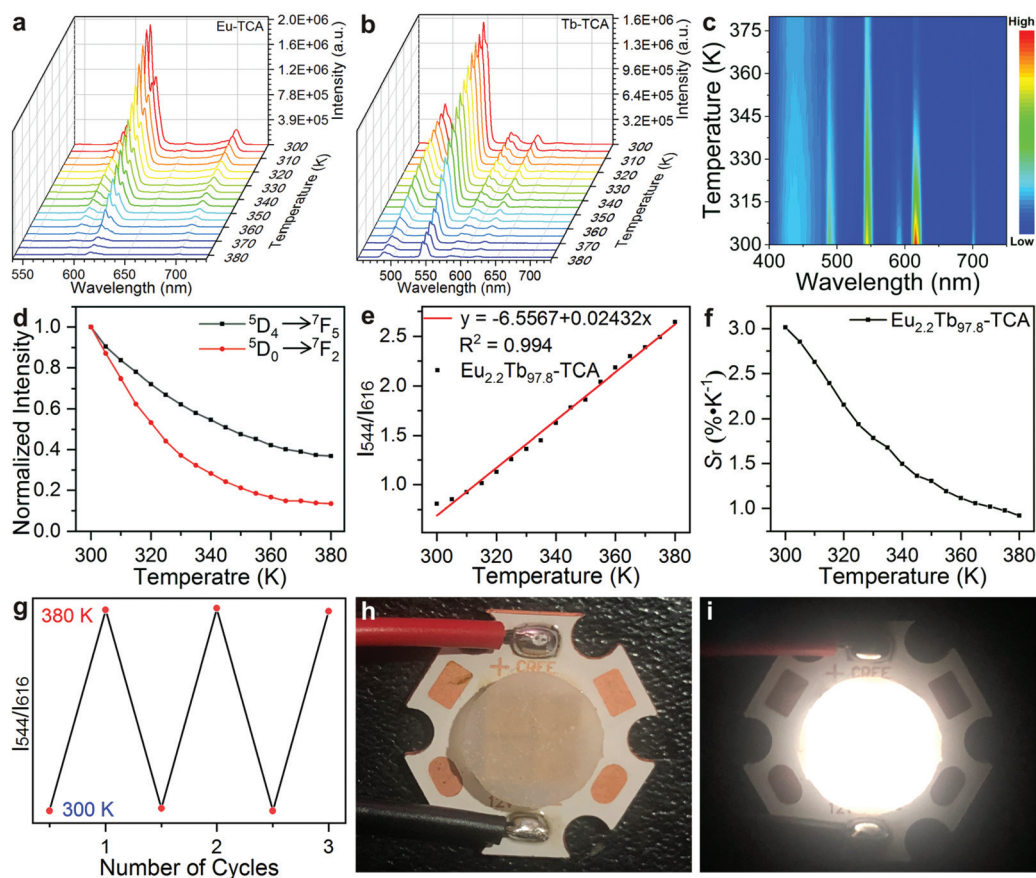


Fig. 4 The luminescence spectra of (a) Eu-TCA and (b) Tb-TCA recorded from 300 to 380 K (excited at 350 nm). (c) Color-coded contour map showing the luminescence spectra of $\text{Eu}_{2.2}\text{Tb}_{97.8}\text{-TCA}$ from 300 to 380 K. (d) Temperature-dependent intensity of the $^5\text{D}_4 \rightarrow ^7\text{F}_5$ and $^5\text{D}_0 \rightarrow ^7\text{F}_2$ transitions in $\text{Eu}_{2.2}\text{Tb}_{97.8}\text{-TCA}$. (e) Luminescence intensity ratio of Tb^{3+} (544 nm) to Eu^{3+} (616 nm) and the fitting curve for $\text{Eu}_{2.2}\text{Tb}_{97.8}\text{-TCA}$ at different temperatures. (f) Relative sensitivity of $\text{Eu}_{2.2}\text{Tb}_{97.8}\text{-TCA}$ in the range of 300 to 380 K. (g) Reversible changes in the relative emission intensities I_{544}/I_{616} of $\text{Eu}_{2.2}\text{Tb}_{97.8}\text{-TCA}$ under alternating cycles at 300 K and 380 K. The luminescent sheet on a four-bead 310 nm LED in the off (h) and on (i) state.

showed a stable ratio after three cycles (Fig. 4g). Thus, $\text{Eu}_{2.2}\text{Tb}_{97.8}\text{-TCA}$ was a good self-calibrating temperature sensor with a good linear relationship, high accuracy and recyclability in a wide temperature range. Theoretically, the E from Tb^{3+} to Eu^{3+} was calculated using the following equation,⁵¹

$$E = (\tau_1^{-1} - \tau_0^{-1}) / \tau_1^{-1}$$

where τ_1 and τ_0 are luminescent lifetimes of the ${}^5\text{D}_4 \rightarrow {}^7\text{F}_5$ transition from the Tb^{3+} (544 nm) of $\text{Eu}_{2.2}\text{Tb}_{97.8}\text{-TCA}$ and Tb-TCA , respectively (Fig. S28†). Moreover, the values of E enhanced upon elevating the temperature from 300 to 370 K, while it decreased in the range of 370–380 K (Fig. S29a†). This phenomenon might be attributed to the phonon-assisted Förster transfer mechanism.⁵² Furthermore, surface-mounted device (SMD) LED lamps were assembled by a mixture of the $\text{Eu}_{2.2}\text{Tb}_{97.8}\text{-TCA}$ phosphor and transparent silicone on a four-beads 310 nm LED and had good-quality white-light emission. Raising the temperature also had not much influence on the white-light emission (Fig. 4h and i). Thus, the as-prepared $\text{Eu}_{2.2}\text{Tb}_{97.8}\text{-TCA}$ can be considered a promising white-light phosphor for fabricating illuminated devices.

3.8. Mechanism of temperature sensing

The luminescence intensity of both Eu^{3+} and Tb^{3+} in $\text{Eu}_{2.2}\text{Tb}_{97.8}\text{-TCA}$ were quenched at elevated temperatures because of the thermal activation of nonradiative decay pathways. To explore this, the lifetimes of the ${}^5\text{D}_4 \rightarrow {}^7\text{F}_5$ transition of Tb^{3+} in Tb-TCA , the ${}^5\text{D}_0 \rightarrow {}^7\text{F}_2$ transition of Eu^{3+} in Eu-TCA and those in $\text{Eu}_{2.2}\text{Tb}_{97.8}\text{-TCA}$ were measured at temperatures from 300 to 380 K (Fig. S28†). The lifetime of Tb^{3+} (${}^5\text{D}_4$) in $\text{Eu}_{2.2}\text{Tb}_{97.8}\text{-TCA}$ was shorter than that in Tb-TCA but longer than that of Eu^{3+} (${}^5\text{D}_0$) in Eu-TCA at the same temperature (Fig. S29b†). This phenomenon indicated that energy transfer from Tb^{3+} to Eu^{3+} occurred. On the basis of Reinholdt's empirical rule,⁵³ the intersystem crossing (ISC) process may be effective when ΔE between the singlet excited-state (S_1) and T_1 of the ligand is higher than 5000 cm^{-1} . The S_1 energy of H_3TCA was $28\,985 \text{ cm}^{-1}$, as obtained from the UV-vis absorption maximum. The T_1 energy of H_3TCA was determined from the solid phosphorescence spectrum of Gd-TCA at 77 K (Fig. S30†) and was calculated to be $20\,964 \text{ cm}^{-1}$ (477 nm). Thus, the energy gap ΔE was determined to be 8021 cm^{-1} , demonstrating that the ISC process was very efficient. Furthermore, ΔE between the T_1 of H_3TCA and Ln^{3+} were 3664 cm^{-1} (for Eu^{3+}) and 464 cm^{-1} (for Tb^{3+}), suggesting that the energy transition from H_3TCA to Eu^{3+} of $\text{Eu}_{2.2}\text{Tb}_{97.8}\text{-TCA}$ was more effective.

4. Conclusions

In summary, the bimetallic Ln-MOF, *i.e.*, $\text{Eu}_{2.2}\text{Tb}_{97.8}\text{-TCA}$, with three visible emissions originating from the two lanthanides and the H_3TCA ligand, was successfully prepared. Benefiting from the two metallic emissive centres, $\text{Eu}_{2.2}\text{Tb}_{97.8}\text{-TCA}$ possessed dual-fluorescence emission under single excitation at

350 nm. Thus, it could act as an efficient ratiometric fluorescent probe for fast real-time (less than 20 s), high-sensitivity (limit of detection 0.016% v/v) and multi-readout detection of water content in the narrow range of 0%–0.63% v/v, as well as an excellent ratiometric fluorescent sensor for temperature determination from 300 to 380 K with high accuracy (3.01%/K at 300 K) and good recyclability. In addition, white-light emission from $\text{Eu}_{2.2}\text{Tb}_{97.8}\text{-TCA}$ was also achieved by adjusting the water content in ethanol. The mechanism revealed hydrogen bonds between H_2O and the nitrogen atoms of the ligands in $\text{Eu}_{2.2}\text{Tb}_{97.8}\text{-TCA}$, which caused sensitive fluorescence changes. Delightfully, by using a smartphone platform, we simply realized visual quantification of water content in a narrow range with a relatively low LOD. Besides, $\text{Eu}_{2.2}\text{Tb}_{97.8}\text{-TCA}$ can also be a promising white-light phosphor for illumination devices with reasonable tuning of temperature. This study paves a new avenue to constructing ratiometric fluorescent sensors with multi-sensing and precise performance for environmental monitoring.

Author contributions

The manuscript was completed through contributions of all authors. All authors have given approval to the final version of the manuscript.

Conflicts of interest

There are no conflicts to declare.

Acknowledgements

We acknowledge the financial support of National Natural Science Foundation of China (Projects 21871121), Science and Technological Plan of Gansu Province (20YF3GA012), and the 111 project (B20027).

Notes and references

- 1 D. Wang, H. Zhao, H. Li, S. Sun and Y. Xu, A fluorescent “glue” of water triggered by hydrogen-bonding cross-linking, *J. Mater. Chem. C*, 2016, **4**, 11050–11054.
- 2 P. Kumar, A. Ghosh and D. A. Jose, Chemical Sensors for Water Detection in Organic Solvents and their Applications, *ChemistrySelect*, 2021, **6**, 820–842.
- 3 Y. Y. Liang, Automation of Karl Fischer Water Titration by Flow Injection Sampling, *Anal. Chem.*, 1990, **62**, 2504–2506.
- 4 H. S. Jung, P. Verwilt, W. Y. Kim and J. S. Kim, Fluorescent and colorimetric sensors for the detection of humidity or water content, *Chem. Soc. Rev.*, 2016, **45**, 1242–1256.
- 5 Y. Zhou, D. Zhang, W. Xing, J. Cuan, Y. Hu, Y. Cao and N. Gan, Ratiometric and Turn-On Luminescence Detection of Water in Organic Solvents Using a Responsive

- Europium-Organic Framework, *Anal. Chem.*, 2019, **91**, 4845–4851.
- 6 A. Douvali, A. C. Tsipis, S. V. Eliseeva, S. P. Petoud, G. S. Papaefstathiou, C. D. Malliakas, I. Papadas, G. S. Armatas, I. Margiolaki, M. G. Kanatzidis, T. Lazarides and M. J. Manos, Turn-On Luminescence Sensing and Real-Time Detection of Traces of Water in Organic Solvents by a Flexible Metal–Organic Framework, *Angew. Chem., Int. Ed.*, 2015, **54**, 1651–1656.
 - 7 L. Chen, J.-W. Ye, H.-P. Wang, M. Pan, S.-Y. Yin, Z.-W. Wei, L.-Y. Zhang, K. Wu, Y.-N. Fan and C.-Y. Su, Ultrafast water sensing and thermal imaging by a metal-organic framework with switchable luminescence, *Nat. Commun.*, 2017, **8**, 15985–15994.
 - 8 T.-I. Kim and Y. Kim, A Water Indicator Strip: Instantaneous Fluorogenic Detection of Water in Organic Solvents, Drugs, and Foodstuffs, *Anal. Chem.*, 2017, **89**, 3768–3772.
 - 9 Y. Zhang, D. Li, Y. Li and J. Yu, Solvatochromic AIE luminogens as supersensitive water detectors in organic solvents and highly efficient cyanide chemosensors in water, *Chem. Sci.*, 2014, **5**, 2710–2716.
 - 10 W.-E. Lee, Y.-J. Jin, L.-S. Park and G. Kwak, Fluorescent Actuator Based on Microporous Conjugated Polymer with Intramolecular Stack Structure, *Adv. Mater.*, 2012, **24**, 5604–5609.
 - 11 X. Du, R. Fan, L. Qiang, Y. Song, K. Xing, W. Chen, P. Wang and Y. Yang, Unusually Flexible Indium(III) Metal–Organic Polyhedra Materials for Detecting Trace Amounts of Water in Organic Solvents and High Proton Conductivity, *Inorg. Chem.*, 2017, **56**, 3429–3439.
 - 12 S. Song, Y. Zhang, Y. Yang, C. Wang, Y. Zhou, C. Zhang, Y. Zhao, M. Yang and Q. Lin, Ratiometric fluorescence detection of trace water in organic solvents based on aggregation-induced emission enhanced Cu nanoclusters, *Analyst*, 2018, **143**, 3068–3074.
 - 13 Y. Huang, W. Liu, H. Feng, Y. Ye, C. Tang, H. Ao, M. Zhao, G. Chen, J. Chen and Z. Qian, Luminescent Nanoswitch Based on Organic-Phase Copper Nanoclusters for Sensitive Detection of Trace Amount of Water in Organic Solvents, *Anal. Chem.*, 2016, **88**, 7429–7434.
 - 14 Y. Dong, J. Cai, Q. Fang, X. You and Y. Chi, Dual-Emission of Lanthanide Metal–Organic Frameworks Encapsulating Carbon-Based Dots for Ratiometric Detection of Water in Organic Solvents, *Anal. Chem.*, 2016, **88**, 1748–1752.
 - 15 X. Liu, Z. Zhou, T. Wang, P. Deng and Y. Yan, Visual monitoring of trace water in organic solvents based on eco-friendly b/r-CDs ratiometric fluorescence test paper, *Talanta*, 2020, **216**, 120958–120964.
 - 16 P. Li, Z. Li and H. Li, Emission Fingerprint Relationships of Low-Level Water in Organic Solvents Based on Ln³⁺- β -Diketonate Complexes in Laponite, *Adv. Opt. Mater.*, 2016, **4**, 156–161.
 - 17 Y.-M. Wang, Y. Xu, Z.-R. Yang, X. Zhang, Y. Hu and R. Yang, Multi-functional lanthanide coordination polymers for multi-modal detection of nitroaromatics and trace water in organic solvents, *J. Colloid Interface Sci.*, 2021, **598**, 474–482.
 - 18 D. Chen, M. Xu, P. Huang, M. Ma, M. Ding and L. Lei, Water detection through Nd³⁺-sensitized photon upconversion in core–shell nanoarchitecture, *J. Mater. Chem. C*, 2017, **5**, 5434–5443.
 - 19 S. Guo, X. Xie, L. Huang and W. Huang, Sensitive Water Probing through Nonlinear Photon Upconversion of Lanthanide-Doped Nanoparticles, *ACS Appl. Mater. Interfaces*, 2016, **8**, 847–853.
 - 20 S. G. Dunning, A. J. Nuñez, M. D. Moore, A. Steiner, V. M. Lynch, J. L. Sessler, B. J. Holliday and S. M. Humphrey, A Sensor for Trace H₂O Detection in D₂O, *Chem*, 2017, **2**, 579–589.
 - 21 L. Yu, Q. Zheng, H. Wang, C. Liu, X. Huang and Y. Xiao, Double-Color Lanthanide Metal–Organic Framework Based Logic Device and Visual Ratiometric Fluorescence Water Microsensor for Solid Pharmaceuticals, *Anal. Chem.*, 2020, **92**, 1402–1408.
 - 22 G. Ji, J. Wang, X. Gao, J. Liu, W. Guan, H. Liu and Z. Liu, Hypersensitive Self-Referencing Detection Traces of Water in Ethyl Alcohol by Dual-Emission Lanthanide Metal–Organic Frameworks, *Eur. J. Inorg. Chem.*, 2018, 1998–2003.
 - 23 H. Li, W. Han, R. Lv, A. Zhai, X.-L. Li, W. Gu and X. Liu, Dual-Function Mixed-Lanthanide Metal–Organic Framework for Ratiometric Water Detection in Bioethanol and Temperature Sensing, *Anal. Chem.*, 2019, **91**, 2148–2154.
 - 24 B. Li, W. Wang, Z. Hong, E.-S. M. El-Sayed and D. Yuan, Ratiometric fluorescence detection of trace water in an organic solvent based on bimetallic lanthanide metal–organic frameworks, *Chem. Commun.*, 2019, **55**, 6926–6929.
 - 25 H. Li, B. Liu, L. Xu and H. Jiao, A hetero-MOF-based bifunctional ratiometric fluorescent sensor for pH and water detection, *Dalton Trans.*, 2021, **50**, 143–150.
 - 26 K. M. McCabe and M. Hernandez, Molecular Thermometry, *Pediatr. Res.*, 2010, **67**, 469–475.
 - 27 X. Wang, O. S. Wolfbeis and R. J. Meier, Luminescent probes and sensors for temperature, *Chem. Soc. Rev.*, 2013, **42**, 7834–7869.
 - 28 Y. Yang, L. Chen, F. Jiang, M. Yu, X. Wan, B. Zhang and M. Hong, A family of doped lanthanide metal–organic frameworks for wide-range temperature sensing and tunable white light emission, *J. Mater. Chem. C*, 2017, **5**, 1981–1989.
 - 29 S.-N. Zhao, L.-J. Li, X.-Z. Song, M. Zhu, Z.-M. Hao, X. Meng, L.-L. Wu, J. Feng, S.-Y. Song, C. Wang and H.-J. Zhang, Lanthanide Ion Codoped Emitters for Tailoring Emission Trajectory and Temperature Sensing, *Adv. Funct. Mater.*, 2015, **25**, 1463–1469.
 - 30 X. Rao, T. Song, J. Gao, Y. Cui, Y. Yang, C. Wu, B. Chen and G. Qian, A Highly Sensitive Mixed Lanthanide Metal–Organic Framework Self-Calibrated Luminescent Thermometer, *J. Am. Chem. Soc.*, 2013, **135**, 15559–15564.
 - 31 Y. Cui, H. Xu, Y. Yue, Z. Guo, J. Yu, Z. Chen, J. Gao, Y. Yang, G. Qian and B. Chen, A Luminescent Mixed-Lanthanide Metal–Organic Framework Thermometer, *J. Am. Chem. Soc.*, 2012, **134**, 3979–3982.

- 32 L. H. Fischer, G. S. Harms and O. S. Wolfbeis, Upconverting Nanoparticles for Nanoscale Thermometry, *Angew. Chem., Int. Ed.*, 2011, **50**, 4546–4551.
- 33 C. D. S. Brites, P. P. Lima, N. J. O. Silva, A. Millan, V. S. Amaral, F. Palacio and L. D. Carlos, Thermometry at the nanoscale, *Nanoscale*, 2012, **4**, 4799–4829.
- 34 C. D. S. Brites, S. Balabhadra and L. D. Carlos, Lanthanide-Based Thermometers: At the Cutting-Edge of Luminescence Thermometry, *Adv. Opt. Mater.*, 2019, **7**, 1801239–1801268.
- 35 (a) T. Xia, Z. Shao, X. Yan, M. Liu, L. Yu, Y. Wan, D. Chang, J. Zhang and D. Zhao, Tailoring the triplet level of isomorphous Eu/Tb mixed MOFs for sensitive temperature sensing, *Chem. Commun.*, 2021, **57**, 3143–3146; (b) J.-W. Liu, X. Han, Y.-T. Lu, S. Wang, D. Zhao and C.-X. Li, Isostructural Single- and Dual-Lanthanide Metal-Organic Frameworks Based on Substituent-Group-Modifying Tetracarboxylate Ligands for Ratiometric Temperature Sensing, *Inorg. Chem.*, 2021, **60**, 4133–4143.
- 36 Y. Cui, R. Song, J. Yu, M. Liu, Z. Wang, C. Wu, Y. Yang, Z. Wang, B. Chen and G. Qian, Dual-Emitting MOF \square Dye Composite for Ratiometric Temperature Sensing, *Adv. Mater.*, 2015, **27**, 1420–1425.
- 37 A. M. Kaczmarek, Eu³⁺/Tb³⁺ and Dy³⁺ POM@MOFs and 2D coordination polymers based on pyridine-2,6-dicarboxylic acid for ratiometric optical temperature sensing, *J. Mater. Chem. C*, 2018, **6**, 5916–5925.
- 38 M. Sekulić, V. Đorđević, Z. Ristić, M. Medić and M. D. Dramićanin, Highly Sensitive Dual Self-Referencing Temperature Readout from the Mn⁴⁺/Ho³⁺ Binary Luminescence Thermometry Probe, *Adv. Opt. Mater.*, 2018, **6**, 1800552–1800558.
- 39 Y. Chen, J. He, X. Zhang, M. Rong, Z. Xia, J. Wang and Z.-Q. Liu, Dual-Mode Optical Thermometry Design in Lu₃Al₅O₁₂:Ce³⁺/Mn⁴⁺ Phosphor, *Inorg. Chem.*, 2020, **59**, 1383–1392.
- 40 X. Wu, S. Zhan, J. Han and Y. Liu, Nanoscale Ultrasensitive Temperature Sensing Based on Upconversion Nanoparticles with Lattice Self-Adaptation, *Nano Lett.*, 2021, **21**, 272–278.
- 41 Y. Shang, Q. Han, S. Hao, T. Chen, Y. Zhu, Z. Wang and C. Yang, Dual-Mode Upconversion Nanoprobe Enables Broad-Range Thermometry from Cryogenic to Room Temperature, *ACS Appl. Mater. Interfaces*, 2019, **11**, 42455–42461.
- 42 T. P. van Swieten, D. Yu, T. Yu, S. J. W. Vonk, M. Suta, Q. Zhang, A. Meijerink and F. T. Rabouw, Ho³⁺-Based Luminescent Thermometer for Sensitive Sensing over a Wide Temperature Range, *Adv. Opt. Mater.*, 2021, **9**, 2001518–2001524.
- 43 M. D. Allendorf, C. A. Bauer, R. K. Bhakta and R. J. T. Houk, Luminescent metal–organic frameworks, *Chem. Soc. Rev.*, 2009, **38**, 1330–1352.
- 44 Y. Jiang, Y. Huang, X. Shi, Z. Lu, J. Ren, Z. Wang, J. Xu, Y. Fan and L. Wang, Eu-MOF and its mixed-matrix membranes as a fluorescent sensor for quantitative ratiometric pH and folic acid detection, and visible fingerprint identifying, *Inorg. Chem. Front.*, 2021, **8**, 4924–4932.
- 45 H.-Q. Yin, J.-C. Yang and X.-B. Yin, Ratiometric Fluorescence Sensing and Real-Time Detection of Water in Organic Solvents with One-Pot Synthesis of Ru@MIL-101 (Al)-NH₂, *Anal. Chem.*, 2017, **89**, 13434–13440.
- 46 L.-L. Wu, J. Zhao, H. Wang and J. Wang, A lanthanide(III) metal–organic framework exhibiting ratiometric luminescent temperature sensing and tunable white light emission, *CrystEngComm*, 2016, **18**, 4268–4271.
- 47 P. Wu, J. Wang, Y. Li, C. He, Z. Xie and C. Duan, Luminescent Sensing and Catalytic Performances of a Multifunctional Lanthanide-Organic Framework Comprising a Triphenylamine Moiety, *Adv. Funct. Mater.*, 2011, **21**, 2788–2794.
- 48 A. Beeby, I. M. Clarkson, R. S. Dickins, S. Faulkner, D. Parker, L. Royle, A. S. D. Sousa, J. A. G. Williams and M. Woods, Non-radiative deactivation of the excited states of europium, terbium and ytterbium complexes by proximate energy-matched OH, NH and CH oscillators: an improved luminescence method for establishing solution hydration states, *J. Chem. Soc., Perkin Trans. 2*, 1999, 493–503.
- 49 Y.-H. Han, C.-B. Tian, Q.-H. Li and S.-W. Du, Highly chemical and thermally stable luminescent Eu_xTb_{1-x} MOF materials for broad-range pH and temperature sensors, *J. Mater. Chem. C*, 2014, **2**, 8065–8070.
- 50 Q. Qiang, S. Du, X. Ma, W. Chen, G. Zhang and Y. Wang, A temperature sensor based on the enhanced upconversion luminescence of Li⁺ doped NaLuF₄:Yb³⁺, Tm³⁺/Er³⁺ nano/microcrystals, *Dalton Trans.*, 2018, **47**, 8656–8662.
- 51 J. Zhou, H. Li, H. Zhang, H. Li, W. Shi and P. Cheng, A Bimetallic Lanthanide Metal–Organic Material as a Self-Calibrating Color-Gradient Luminescent Sensor, *Adv. Mater.*, 2015, **27**, 7072–7077.
- 52 Y. Liu, G. Qian, Z. Wang and M. Wang, Temperature-dependent luminescent properties of Eu–Tb complexes synthesized *in situ* in gel glass, *Appl. Phys. Lett.*, 2005, **86**, 071907–071910.
- 53 M. O. Rodrigues, J. D. L. Dutra, L. A. O. Nunes, G. F. de Sá, W. M. de Azevedo, P. Silva, F. A. A. Paz, R. O. Freire and S. A. Júnior, Tb³⁺→Eu³⁺ Energy Transfer in Mixed-Lanthanide-Organic Frameworks, *J. Phys. Chem. C*, 2012, **116**, 19951–19957.